IJS Internal Report
IJS-DP-9988
Date: July 2008

MCNPX / MCNP5 ROUTINE FOR SIMULATING D–T NEUTRON SOURCE IN Ti-T TARGETS

Author: Alberto Milocco

Supervisor: Andrej Trkov

Institut »Jožef Stefan«, Ljubljana, Slovenija

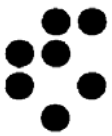

MCNPX/MCNP5 ROUTINE FOR SIMULATING D–T NEUTRON SOURCE IN Ti-T TARGETS

1. Introduction

The benchmark experiments on fusion neutronics rely on 14 MeV neutron sources. High yields of source neutrons are usually generated by accelerating deuterons onto solid Tritium–Titanium targets. Thus, the $^{3}H(d,n)^{4}He$ reaction is used in the experimental facilities. The neutron source specification is a starting-point for the analysis of benchmark experiments and for the uncertainty assessment. Integral experiments for fusion technology have been collected in the International Database for Integral Shielding Experiments (SINBAD). The database makes available two source routines that claim to include the engineering and physical features of the neutron generators. The ORNL produced an oversimplified modelling of the D–T source. The source routine developed at ENEA is the most realistic and is described here. It is inserted in the SOURCE subroutine of the MCNP5 original source code. It is based on the 'Stopping and Range of Ions in Matter' code (SRIM2006, http://www.srim.org/). SRIM is a well established collection of software packages (TRIM is the for ion transport) that calculate many features of the transport of ions in matter, as ion stopping and range in targets, ion implantation, sputtering, ion transmission, ion beam therapy. SRIM was developed since the 90's by J. F. Ziegler, J. P. Biersack and M. D. Ziegler. M. Pillon, the author of the ENEA source routine, translated into Fortran language the statements of an old version (1996) of TRIM written in basic language for the modelling of the D-ion transport inside the target. There is a strict parallelism between the source routine and the TRIM old version. M. Pillon dropped the part concerning the target damage and implemented the original part concerning the neutron production. This report is an extreme synthesis of the physics and the computational techniques contained in the source routine. Chapter 2 deals with the D-ion transport inside the target. Besides some explanations by the author M. Pillon, the description is based upon the SRIM manual [1]. The reliability of the model is assessed by comparing the results of the source routine with that one from the TRIM code. Chapter 3 presents the analytical issues involved in the fusion reaction. Minor improvements have been introduced to the original version of the source routine and they are discussed. An Appendix was added for mathematical derivations and details. The neutron spectrum that is generated by the source routine is then validated (chapter 4) versus measurements performed at the ENEA Frascati Neutron Generator (FNG) and at the JAERI Fusion Neutronic Source (FNS). The conclusion aims at underlining the importance of having a reliable source routine for the analysis of integral benchmark experiments.

2. The deuteron transport

As Bohr suggested in 1913, it is convenient to divide the energy loss of an ion in matter into the energy losses to the heavy target nuclei (elastic scattering), and to the target electrons (inelastic scattering). While an ion passes through the material, the stationary nucleus recoils and absorbs energy and the moving particle is deflected. The final velocities and trajectories can be found simply from the classical conservation of angular momentum and energy of the system. Mathematically this problem is called the 'asymptotic orbit problem'[a] and it has analytical solutions for simple central potentials between the particles.

[a] The classical treatment of elastic scattering may be valid over a wide range of angles, say $\theta > \theta_c > 0$, even for potentials of infinite range. Without a detailed analysis, uncertainty principle arguments may be used to estimate

The transfer of energy from the ion to the atom is complicated by the complex electronic screening of the two nuclei and the physics of quantised collisions between atoms, for example the shell effects and the absorption of energy into the Pauli promotion of the electrons. In general, the potential field of the two nuclei, called the 'interatomic potential' $V(r)$ (r being the radial coordinate), can be considered as a coulombic term (Ze/r, due to charge Ze) multiplied by the 'screening function' (Φ):

$$\Phi = \frac{V(r)}{(Ze/r)} \tag{1}$$

There are three approaches to calculate the screening function and hence the interatomic potential. One way is to use experimental data and try to work back to the potential. The second one is to incorporate full quantal treatments for all electronic collisional interactions. The third approach is to isolate a few interactions of importance to energetic collisions and to estimate the potential from limited calculations. The latter approximation is the one implemented in the source routine. It takes into account from one side the coulombic interaction between all the electrons and the two nuclei and from the other the increased quantal energy that goes into excitation and exchange effects for the electrons in the volume of atomic overlap. The major assumption is that the local electron distribution remains fixed without any reconfiguration of the atomic structures as a whole. The main attraction of this procedure is that it can be applied to any combination of atoms (it is 'universal'), with the only input being the two charge distributions. When comparing the results involving many collisions to those of detailed and much more complex calculations, the error is acceptable for interatomic potentials above few eV. This corresponds to the general experience in quantum mechanics that accurate values for the change in energy can be obtained without changing the electronic distribution in the sense of the first order perturbation theory[b]. Traditionally, the radial abscissa r is restated as the reduced radius, x, which is the atomic radius divided by the 'screening length', a. This important parameter is inserted into the potential in order to increase the size of an atom by moderating the effect of the nuclear positive charge because the inner electrons shield some of the nuclear charge. In other words, it describes the radial gradient of the potential, so also effects coming from surrounding atoms can be included. By adopting the 'universal screening length' defined as:

---

the value for the critical angle θ_c for the validity of the classical analysis. A particle of angular momentum $lh/2\pi$ and momentum $k=\mu v_0$ initially along the x-axis must be tought as a narrow wave packet with transverse spread Δy in position, ΔV_y in y component of velocity. If $\Delta\Phi$ is the angular spread, then $\Delta V_y \sim v_0 \Delta\Phi$. The concept of an orbit will be meaningful only if $\Delta\Phi$ is negligible compared with the polar angle Φ of the particle's position vector $r=(r,\Phi)$, that is $\Phi >> \Delta V_y/v_0$. The uncertainty principle requires $\mu\Delta V_y \Delta y >> h/2\pi$ or $\Delta V_y >> h/(2\pi\mu\Delta y)$ so that the requirement is: $\Phi >> h/(2\pi\mu\Delta y)$. Writing $l= (2\pi\mu\Delta y)/h$, one obtaines $\Phi >> 1/l$. This simple argument shows that $\theta_c >> h/(2\pi L)$ where L is the classical orbital momentum. Typically for electron impact L is of order a few times $h/2\pi$, and $\theta_c \sim 1$ radian $\sim 60°$, so the range of validity of classical mechanics is small. However for proton (or deuteron) impact, even at thermal velocities, μ is of order 10^3 m_e so that L is of order 10^3 $h/2\pi$ and $\theta_c \sim 10^{-3}$radians $\sim 0.1°$ [2].

[b] This universal screening function has been further reviewed by comparing 106 experimentally determined potentials with the universal ones. The overall standard deviation between theory and experiment is 5%. Good agreement was obtained also in the comparison between the proposed formulation presented here and the full orbital scattering integral. Discrepancies as large as 5% exist. However, discrepancies so large are the exception rather then the rule. Detailed examination indicates most differences are 2% or less and the mean deviation is 2.1%. This quality of the agreement between the fitted results and the detailed calculations over at least 9 orders of magnitude in energy is considered quite satisfactory, and since it asymptotically approaches the proper limit for high energies, this provides some justification of the detailed 5 parameter formulation (see later equation 7).

$$a_u = 0.8854 a_0 / (Z_1^{0.23} + Z_2^{0.23}) \qquad (2)$$

where a_0 is the Bohr radius, the interatomic potential is independent on the ion-target combination and yields the 'universal potential':

$$\Phi_u = 0.1818\ e^{-3.2x} + 0.5099\ e^{-0.9423\ x} + 0.2802\ e^{-0.4028\ x} + 0.2817\ e^{-0.2016\ x} \qquad (3)$$

Moreover, it is convenient to introduce the reduced CM energy ε, the reduced impact parameter b and the reduced distance of closest approach R_0

$$\varepsilon = \frac{aE_c}{Z_1 Z_2 e^2} \qquad b = \frac{p}{a} \qquad R_0 = \frac{r_0}{a} \qquad (4)$$

to obtain the scattering trajectory or scattering integral in a universal way:

$$\theta = \pi - 2 \cdot \int_{R_0}^{\infty} \frac{b\,dx}{x^2 \left[1 - \frac{\Phi(x)}{x\varepsilon} - \frac{b^2}{x^2} \right]^{1/2}} \qquad (5)$$

Now, some straightforward nomenclature: the final angle of scatter in the cm system, θ, is evaluated in terms of the initial CM energy E_C, the impact parameter p, the distance of closest approach r_0 and the screening function. The previous equation is used to calculate[c] the energy transferred to the target atom. The following equation is implemented:

---

[c] But also:

- The energy lost by the ion per unit path length. This is related to the nuclear stopping cross section, $S_n(E)$, by the relation $dE/dR = NS_n(E)$, where N is the atomic density of the target. The nuclear stopping power is the average energy transferred when summed over all impact parameters, that is, in reduced units:

$$S_n(\varepsilon) = \int_0^{\infty} T d\sigma = \varepsilon \int_0^{\infty} \sin^2 \frac{\theta}{2} db^2$$

In the source routine the nuclear stopping power data are retrieved from the SR module of the SRIM code and copied in the data section. Since SRIM is considered a reliable source of information, further details are not here provided, addressing the interested reader to [1].

- The nuclear straggling. The study of particle straggling begins with deriving Bohr straggling, which is the straggling between a moving charged particle and a stationary charged particle, in the limit of non – relativistic Coulomb interactions. The units of straggling are [(energy loss)^2/distance]. The straggling of two particle energy loss is defined as the second momentum of T, the energy loss to the stationary particle:

$$Q_2 \equiv \frac{(\int_0^{\infty} T^2 d\sigma)/\sigma}{<\Delta x>} = \pi \gamma Z_1^2 e^4 M_1 / (<\Delta x> M_2 \sigma) \qquad ; \qquad \gamma = 4 M_1 M_2 / (M_1 + M_2)^2$$

Where $<\Delta x>$ is the average distance travelled by the projectile. Bohr extended this formalism to the ion – electron energy loss case. Assuming a target with atomin density N, atoms/cm^3, with Z_2 electrons/atom, then the mean distance between collisions is $<\Delta x> = 1/N\sigma$ and this final equation is obtained, which is used in the source routine: $Q_2 = 4\pi e^4 Z_1^2 Z_2 N \cdot \Delta x$

$$T = \frac{4E_C M_c}{M_2}\sin^2\frac{\theta}{2} = E_0\gamma\sin^2\frac{\theta}{2}\ ; \qquad \gamma = 4M_1M_2/(M_1+M_2)^2 \tag{6}$$

where T and E_0 are the energy transferred and the initial energy of the ion in the lab system. Authors in the field have long sought to replace the scattering integral with some analytical or numerical equivalent, which is indeed a major simplification, but necessary. The approach here considered was proposed by Biersack and Haggmark (1980). Their solution involves no approximation other than the validity of scattering integral. They suggested that the centre-of-mass scattering angle has the following relation:

$$\cos\frac{\theta}{2} = \frac{b + R_C + \Delta}{R_0 + R_C} \tag{7}$$

With other two reduced quantities:

$$R_C = \frac{\rho}{a} \text{ and } \Delta = \frac{\delta}{a} \tag{8}$$

where Δ is a correction term that is empirically fitted. The term ρ describes the radius of curvature of the two particles at the point of closest approach and is calculated from:

$$\rho = -2\left[E_C - V(r_0)\right]/V'(r_0) \tag{9}$$

and $V'(r_0)$ is the spatial derivative of the interatomic potential at point r_0. All of these terms are straightforward to calculate. This formula allowed for the first time a quick solution to the scattering problem with high precision, instead of having to do the complete evaluation of the scattering integral. The authors called it the 'Magic Formula'. In the high-energy limit, atomic collisions can be adequately described using the unscreened Coulomb interatomic potential, i. e. Rutherford scattering. Therefore, the formula for Δ asymptotically approaches the Rutherford result as ε becomes large. Indeed, even though the above formulation has built in validity for large ε, it is more efficient to base the calculations directly on the Coulomb potential for ε>10. To include the electronic screening effect near the nucleus (varying from an r^{-1} through an $r^{-1.5}$ to an r^{-2} potential the expression for the Rutherford scattering is corrected by the term in square brackets in the following expression:

$$\sin^2(\theta/2) = 1/\left\{1 + \left[1 + b(1+b)\right](2\varepsilon b)^2\right\} \tag{10}$$

While the ion travels between the sites of nuclear collisions, it continuously loses energy due to the inelastic scattering with the electrons of the medium. The stopping power data of deuterons dE/dx in Titanium and in Tritium, in both nuclear and electronic components, are retrieved from the SR module of SRIM code and inserted into the data

section of the source routine. The rich literature on the stopping power allows confidence on the data inserted into the source routine. Thus, attention is paid on the internal processing of the stopping power data. Assuming that the energy loss in a compound is the sum of the energy loss in its constituents (Bragg's law), the rate of energy loss of deuterons in a Ti–T target is given by[d]:

$$(dE/dx)_{Ti-T} = \frac{A_{Ti}}{A_{Ti} + A_T a_f}(dE/dx)_{Ti} + \frac{A_T a_f}{A_{Ti} + A_T a_f}(dE/dx)_T \qquad (11)$$

Where A_{Ti}, A_T and a_f are the atomic weight of Ti, the atomic weight of T and the atomic fraction T/Ti respectively. The effect of the atomic fraction is illustrated in Figure 1.

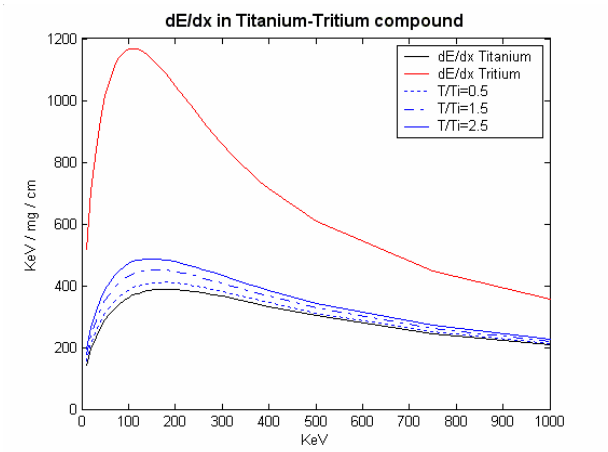

Figure 1. dE/dx in Ti, T, and compounds

By interpolating the total stopping power at the D-energy before next collision, the deuteron energy loss ΔE in the interval Δx between two successive collisions is calculated by the following formula:

$$\Delta E = \frac{dE}{dx}\Delta x \qquad (12)$$

ΔE is then corrected by the Bohr straggling effect (see note c).

For the computer simulation of the slowing down and scattering of ions in materials, the Monte Carlo method as applied in simulation techniques has a number of distinct advantages over analytical formulations based on transport theory. For instance, it allows more rigorous treatment of elastic scattering. Ziegler's method begins with a given energy, position and direction. The particle is assumed to change direction because of binary nuclear reactions and move in straight free-flight-paths between collisions. Thus, particles lose energy in discrete amounts in nuclear collisions and lose energy continuously from electronic

[d] The original source routine contained an error at this point due to a change in units between successive versions

interactions. The nuclear scattering determines the spatial distribution of particle trajectories. A history is terminated either when the energy drops below a specified value or when the particle position is outside the target[e]. The target is considered amorphous with atoms at random locations. The selection of the target atom is performed by random numbers, assuming the probabilities of encounters being proportional to their stechiometric abundance[f]. This method is applicable to a wide range of incident energies from approximately 0.1 KeV to several MeV, depending on the masses involved. The lower limit is due to the inclusion of binary collisions only, while the upper limit results from neglecting relativistic effects. The CPU calculation time is reduced by omitting the calculation of collisions that transfer 'negligible' amounts of energy and cause 'negligible' deflection angles in the ion trajectory[g]. When the ion skips over many monolayers, such quantities as electronic energy loss are still spread properly into these layers. A criterion is set up as a minimum energy transfer to calculate the maximum distance the ion can jump (without collisions) until there must be a significant collision. The method of calculating the free–flight–path (*FFP*) is straightforward if the traditional 'impulse approximation' is used, which is applicable whenever $T<<E$, or the scattering occurs with $sin^2\theta<<1$. The impulse approximation was first studied extensively for Coulomb collisions. The conclusion was that $sin^2\theta$, and also T by equation 6, can be reduced to a simple relationship with the impact parameter of the collision. An approximation of this solution was obtained for the universal potential by using the expression:

$$p_{\max}/a = b_{\max} = (\xi + \xi^{0.5} + 0.125\xi^{0.1})^{-1} \qquad \xi = (\varepsilon\varepsilon_{\min}/\gamma)^{0.5} \tag{13}$$

Here ε_{min} is the reduced minimum energy transfer T_{min}, below which any energy transfer is considered negligible. At high energies ($\varepsilon>>10$) even over distances large compared with the interatomic distance in a solid, a noticeable deflection is a rare event and it is connected with a very small impact parameter. This method has the advantage of extending the *FFP* at higher energies, thus saving further computer time. Assuming that there is one target atom in cylinder of volume N^{-1}, the maximum *FFP* is calculated by this equation:

$$\pi(p_{\max})\cdot FFP = N^{-1} \tag{14}$$

The *FFP* is not a constant length, for once the maximum jump distance is estimated, this length is reduced by a random number (ranging from 0 to 1) to distribute the probability of the collision to somewhere randomly within the jump length. So the *FFP* for random collisions is made such that the total mean energy transfer of all intermediate collisions is less then T_{min}. In calculations of sputtering or damage production, the low energies are to be treated quite precisely. In collision cascades, for example, the recoils are followed through

[e] The thickness condition was not present in the original version of the source routine. It is inserted by terminating the Monte Carlo history when the cumulative deuteron free flight path exceeds the target thickness

[f] This is by no means trivial, and actually it was a matter of some concern whether lighter atoms could have a smaller cross section than havier ones. Trims lets the potentials to take care of the situation without imposing any arbitrary cut-offs for lighter atoms as compared to havier ones. This means that TRIM allows interactions at equally large impact parameters for all target atoms, but expects, for example, at a given large impact parameter that a light target atom with a lower interaction potential will cause only minimal deflection and lower energy transfer as compared to a heavier component. The difference between a light and heavy target turns out to lie in the magnitude of the potential, but not in the range of interaction.

[g] The definition of negligible in TRIM is any random quantity (non cumulative) which has less then 0.1% effect on the final results.

several generations until their energies typically reach E_s=3-6 eV or E_d=15-30 eV. The approach depicted above is indeed a simplification of the TRIM code, which posed conditions that change the simple pattern in order to get results that are more accurate. Dramatic discrepancies are not expected in the deuteron transport as performed by TRIM or by the source routine that is based on the description above, except from some features that are described below. The analytical tools for a proper comparison have been implemented in a test version of the source routine and on MATLAB functions in order to compare:

A) the ion average range
B) the collision density
C) the ion energy distribution across the surfaces inside the target.

The starting D-energy is 280 KeV and the Ti/T atomic ratio is one. The threshold energy value for the history termination is 10 KeV.

Case A) TRIM is an established code for reference range calculations. Its result is 1.59 μm of D average range in the Ti-T target in the forward direction. The same information was retrieved from the test version of the source routine. This calculation provides the D average range of 1.51 μm. Thus, the agreement can be considered fair.[h]

Case B) Retrieving information on the ion energies is indeed not simple in TRIM, because the major objective of the code is to compute the damage produced in the target. The author explained that the output file EXYZ was an after-thought, which was not intended to yield much physics. Anyway, once properly interpreted and used, it contains the printouts of the ion energy after any collision. A consistent file was generated from the test version of the source routine and the energies after any collision are binned in a very fine energy mesh (10 KeV) until the D-energy drops below 10 KeV. In the current TRIM code some features seem to be implemented differently as in the source routine. There is a special treatment in TRIM for the first collision of the surface layer of the target. When implemented in the source routine it caused an anomalous spike at maximum ion energy in the ion collision density. Ziegler advises TRIM users that such kind of peaks can occur due to the *FFP* approximation. Three ways to overcome the problem were considered.

- Averaging over larger bins: the 10 KeV binning is indeed more academic then realistic, considering the instrumental energy resolution.
- Using the monolayer distance instead of the FFP as the unit for the ion travel between collisions. This option has two major drawbacks: the computational times are increased by a factor 10-50x and a proper comparison between the source routine and TRIM could not be achieved based on the EXYZ file.
- Dropping the first collision, which is based on the monolayer distance, in the source routine.

M. Pillon implemented the latter choice in the source routine. The D-energy distributions obtained from the source routine and from TRIM are compared in Figure 2. Neglecting the first collision in the source routine explains why at the higher energies the ion energy distribution is smoothed out. Another major approximation in the source routine was observed. The maximum FFP is not randomized in the source routine, but only the energy after the collision is. From this point, the new energy of the deuteron is not a random value but the minimum energy of the ion, i. e. corresponding to maximum energy loss. The aim of the subroutine was not to calculate the range or position of the ion, but only the energy distribution of the ions. Following strictly the rule described before, that is considering the *FFP* as obtained by multiplying the maximum *FFP* for a random number, and assigning the

[h] A much grater discrepancy was found in the original source routine because of the mistake in the dE/dx quoted above.

energy based on the random *FFP* to the ion after the collision, a better agreement was found in the D-collision density (Figure 3). In this case, the special treatment of the first collision was maintained and its effect is to some extent comparable to TRIM. Moreover, the number of collisions that are necessary to slow down the deuteron to 10 KeV agree in this second case with TRIM calculation, whereas the approach of Figure 2, as one can expect, requires on the average half of such collisions.

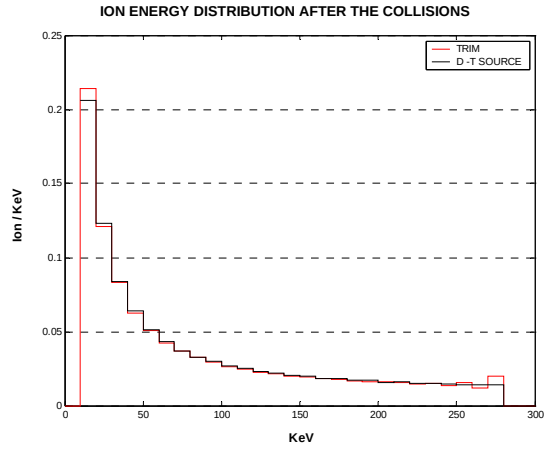

Figure 2. Collision density in source routine

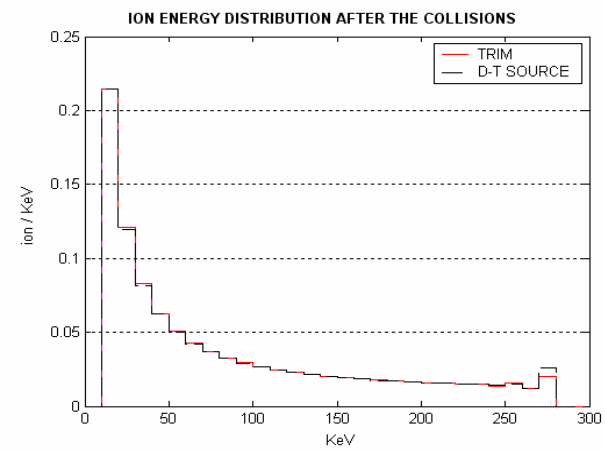

Figure 3. Collision density after FFP modification and first collision accounting

This insight into the slowing down process does not allow choosing the second modelling of the ion collisions because in this case the TRIM manual is the only reference, whereas the old source subroutine was based on the TRIM basic coding. The new version of the TRIM source code is not available and arguing that the old version has to be changed in this way is somewhat arbitrary. The main concern arose because of the spike at the maximum energy. With Pillon's suggestion no spike arises anymore and the ion spectrum does not differ dramatically from the reference TRIM spectrum. It is worthwhile to notice at this point another difference between TRIM and the source routine. In the source routine the default value of T_{min} is 5 eV. This value clearly affects the D-spectrum and it was chosen in order to minimise the differences between the signals obtained with TRIM and with the source routine.

Case C) TRIM provides the output file TRANSMIT that prints the energies of the ion when crossing the edge of the target. This file was reproduced as well in the test version of the source subroutine by inserting an original condition on the target thickness. The Monte Carlo history is terminated when the cumulative deuteron free flight path exceeds the target thickness. When an ion approaches the target edge, TRIM shortens the flight paths. This feature is not implemented in the source routine. In the latter, the energy of the deuteron is printed out when its distance exceeds the target thickness. The target thickness was set at 0.5 μm and 1 μm. The energies of the transmitted D were then binned in energy regardless of directions. The printouts from TRIM and from the source routine are compared. As explained above, the comparison has to be considered quite generic. Nevertheless, from Figures 4 and 5 the agreement is still good for our purpose, which is not related to ion positions.

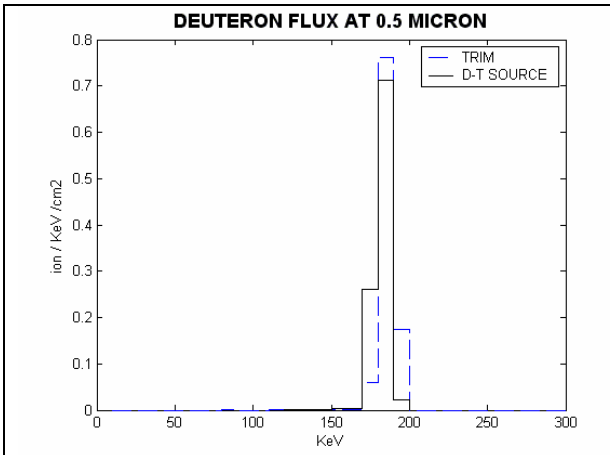

Figure 4: Spectrum of D transmitted at .5 μm

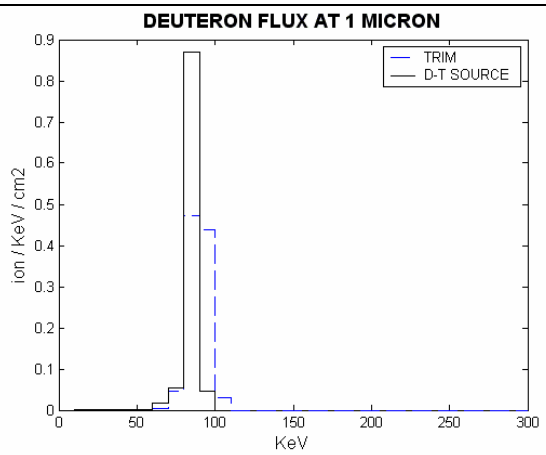

Figure 5. Spectrum of D transmitted at 1 μm

3. Neutron production

In order to generate a neutron, the source routine models the theoretical $^{3}H(d,n)^{4}He$ reaction at the D-energy after any nuclear collision. Since the probability of an interaction with the Ti or T atom depends only on the stechiometric abundances, this would not affect the neutron spectrum, but only the total neutron yield. The ratio of the elastic over the total cross section of T and the ratio of the fusion over the total cross sections of T can play different rules at different D-energies and neutron emission angles. This matter is not addressed in the source routine. Indeed, it is cumbersome to stack this treatment into the TRIM model of nuclear scattering. This paragraph describes the way neutrons are generated given the D-energy as above obtained. At the end, any neutron is generated at the front surface of the target, at an energy and direction in the laboratory system. It is then transported by means of the MCNP5 code. The statements for the D-transport inside the target and for the neutron production are implemented in the SOURCE subroutine of the MCNP5 source code. The SRCDX subroutine is required for transporting the neutron to point detectors. Other subroutines are added for numerical calculus. A patch file was created to apply to the original MCNP5 source code for the UNIX shell of WINDOWS (Cgywin). To this purpose the 'Depends' and 'List' files were modified for inclusion of the new MCNP5 subroutines. The D-T source was also compiled in a UNIX machine for parallel mode, but it does not work with point detectors. Point detectors are usually not required in long runs. The MCNP5 code with the source routine allows the calculation of the neutron spectra at any direction. The use of the RDUM card is required in the MCNP5 input file to specify: deuteron beam energy, target thickness, T/Ti atomic fraction, beam width and target axis coordinates.

Let *P(E)dE* denote the probability that $^{3}H(d,n)^{4}He$ reaction occurs in the Ti–T target at D-energy *E* around interval *dE*.

$$P(E)dE \propto \sigma(x)\Phi(x)n_T(x)dx = \sigma(E)\Phi(E)n_T(E)\frac{dx}{dE}dE \qquad (15)$$

where $\Phi(E)$ is the deuteron flux, $\sigma(E)$ the cross section of the D–T reaction, dE/dx is the stopping power. $n_T(E)$ is the target atomic density, which is considered constant. In equation (15) it is still assumed that the reaction products are emitted isotropically in the CM system. In the general case of anisotropic neutron distribution, the following reaction probability has to be considered:

$$P(E,\omega) \propto \sigma(E,\omega)/(\frac{dE}{dx})\Phi(E) \tag{16}$$

where $\sigma(E,\omega)$ is the double differential cross section. In the original source routine the double differential cross sections in an energy and angle grid were inserted into the code data section. This table was retrieved from from DROSG200 code calculations. The code was developed by M. Drosg. It is available at the IAEA Nuclear Data Section (http://www-nds.iaea.org/drosg2000.html) [3]. This approach has two drawbacks. First, it is not easy to check if any data is wrong or approximate because the amount of data is huge. Second, the xs data rely on DROSG2000 Legendre coefficients, which can change according to new experimental evidence or refinement of theoretical nuclear models. The proper source of information for the double differential cross sections is the ENDF file for the ^{3}H(d,n)^{4}He reaction in the ENDF/B-VI nuclear data library (MAT=2, MF=50, MT=3,6 [4]). The Legendre coefficients are the only information needed to calculate the cross sections at each D energy and neutron emission angle in CM system. Thus, a set of procedures were implemented for generating internally the Legendre polynomials and the cross sections from the Legendre coefficients up to the tenth order, copied into the data section. The answers of the original source routine and the new one have been compared. The neutron spectra are calculated with MCNP5 at different angles from 0 to 180 degrees in void. The energy binning is 10 KeV. The MCNP output is processed with the ACEFLX code developed by A. Trkov at IJS. The deuteron energy is 280 KeV. The other parameters in the RDUM card are set to their standard values: the beam width is 0.7 cm, Ti/T atomic ratio is 1.5 and target thickness is 0.001 cm. The slight difference (Figure 6) between the old and the new cross sections involved a small difference in the scaling factors (~5%). Except for this detail, the distributions at each angle agree.

The source routines were further implemented to introduce the relativistic kinematics, whereas the original source routine used the classical approach [5]. The neutron energy is calculated from the following formulas:

$$P_1 = \left\{(E_a+m_b)^2 - P_a^2\cos^2\theta_1\right\}^{-1}\left[\ P_a\cos\theta_1\left\{m_bE_a+\frac{1}{2}\left(m_a^2+m_b^2+m_1^2-m_2^2\right)\right\}+\right.$$

$$\left.+\left(E_a+m_b\right)\left[\left\{m_bE_a+\frac{1}{2}\left(m_a^2+m_b^2-m_1^2-m_2^2\right)\right\}^2 - m_1^2m_2^2 - m_1^2P_a^2\sin^2\theta_1\right]^{\frac{1}{2}}\ \right] \tag{17}$$

$$\frac{d\Omega_{CM}}{d\Omega_{LAB}} = K\frac{P_1^2}{(E_a+m_b)P_1 - P_aE_1\cos\theta_1} \tag{18}$$

The nomenclature and the demonstration of these equations are reported in Appendix A1. The effect of the relativistic approach is represented by the neutron spectrum shift toward lower energies of about 30 KeV as can be seen in Figure 7. To calculate the mean values of the neutron energy and the yields at different angles a MATLAB function was developed which reads from ACEFLX output. Thanks to the thickness condition described above the target thickness is changed. In the limit of a very thin target (0.1 μ) the neutron mean energy and yields at different angles converge to the theoretical ones since little deuteron slowing down and deflection occur. In Figure 7–8 the latter is indicated by crosses, which agree very well in the case of the ultra thin target. This also confirms that the neutron energies and angles are properly calculated.

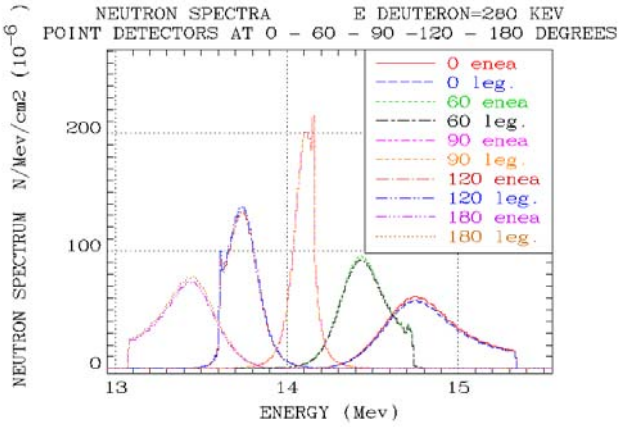

FIGURE 4. Neutron spectra with xs from ENDF/B-VI Legendre coefficients

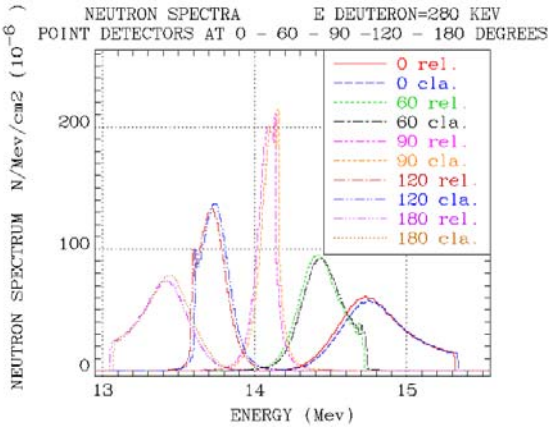

FIGURE 5. Effect of relativistic kinematics

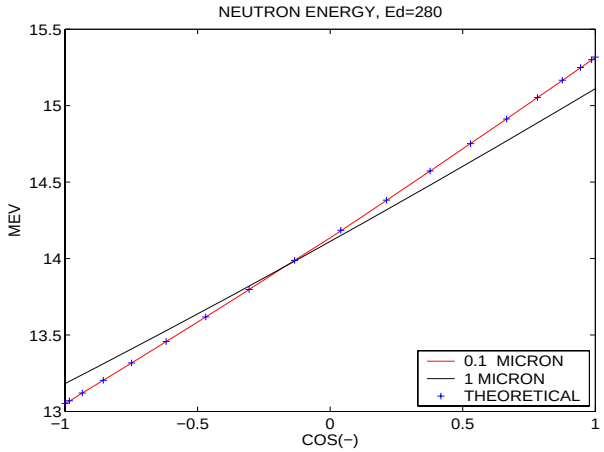

FIGURE 7. Target thickness effect on energy

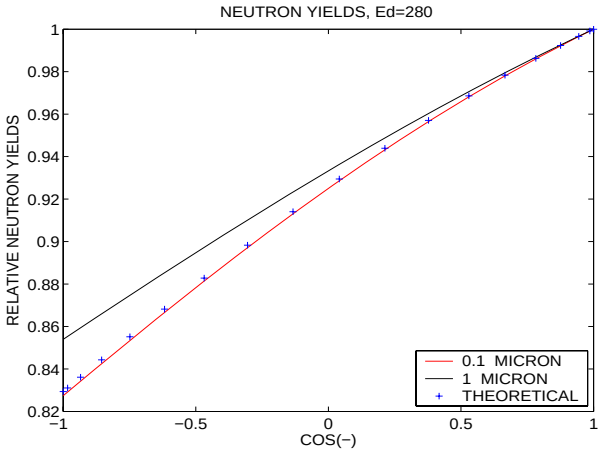

FIGURE 8. Target thickness effect on yields

The extraction of a random variable from the probability density function is performed with a rejection method (see Appendix 2). The polar angle is sampled uniformly. The emission in the azimuthal angle is assumed uniform. The neutrons are produced in CM frame and subsequently their direction is transformed into the target frame. The SRCDX subroutine

retrieves the direction and energy of the neutron generated in the SOURCE subroutine trough the common block. The contribution to each point detector is weighted according to the anisotropy of the neutron distribution. This involves integrations of the angular distributions, which can explain the slight differenced in Figure 4. The point detector flux estimator is very useful with the bare source. The modifications described implied a revision of the SRCDX subroutine for point detectors. A cross-validation of the source model code is performed comparing the MCNP cell flux estimator (CF) and the point detector (PD) signals. It can be inferred (Figure 9) that both tallies are consistent, except from some fluctuations in the cell flux estimator. The energy range starts at the theoretical neutron energy. The energy spread is greater in the forward direction. The shape of the neutron spectra can be explained by considering that the maximum of the $^{3}H(d,n)^{4}He$ integral cross section is at 109 KeV.

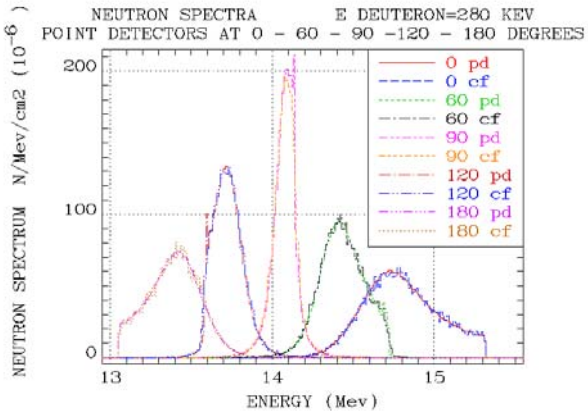

FIGURE 9. Cross validation of tallies

4. Validation

An experiment that was carried out at FNG with the bare ~14 MeV neutron source configuration was considered an ideal test case for the source routine validation. It consisted of a study of the characteristics of a type IIa diamond detector [6]. The experimentalist M. Pillon provided the raw experimental data, which are the counts per channel of the measurement. The transformation into the energy spectra was performed applying the calibration formula and an energy shift of 5.7 MeV due to the kinematics of the $^{12}C(n,\alpha_0)^{9}Be$ reaction in the diamond detector. A detailed MCNP model of the FNG neutron generator and experimental room was used to reproduce the measured spectrum using point detectors at the diamond detector positions at 0°, 95° and 172.5°. The energy of the accelerated D is 230 KeV M. Pillon also provided the output file of the MCNP5 calculation carried out with the original source routine. Thus, the spectra obtained with the current source routine are compared both with the ones retrieved from Pillon's output file and with measurements (Figure 10). The tails in the measurements below the ~14 MeV peak are due to the incomplete charge collection in the diamond detector, which cannot be reproduced with the point detectors in MCNP5. A 1 % FWHM Gaussian broadening was applied to calculated signals. The spectra are normalised to the maxima of the measured spectra and the same scaling factors are applied to the calculated signals by old and new version of the source routine. The energy binning is finer in the latter

case, as can be seen for the 172.5° spectra. In the backward direction, the source routine provides spectra somehow shifted towards higher energies. The shapes of the calculated peaks are in fair agreement with the measured ones. The spectrum calculation in the forward direction is preferable after the improvements implemented in the source routine.

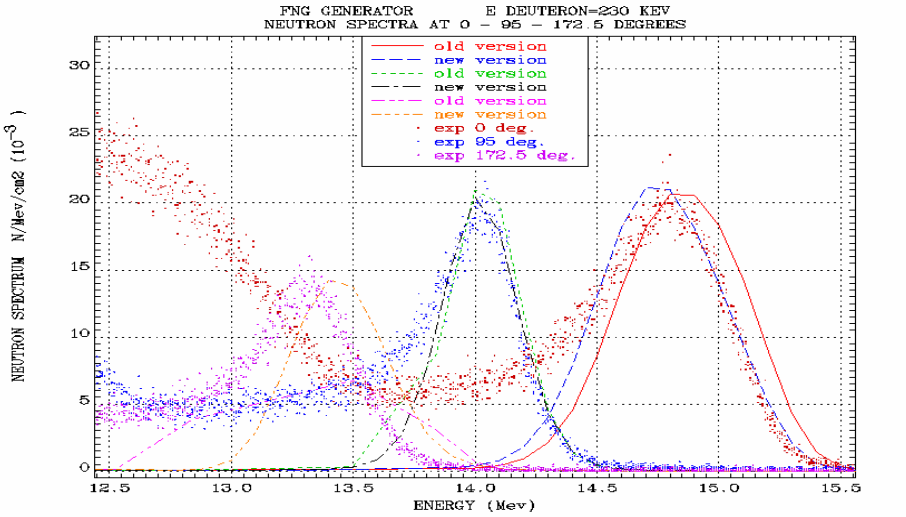

FIGURE 10. Diamond detector spectra simulations

The present study of the source routine was carried out with the intention to make a general use of it, which is to apply it also to other neutron generators. An experiment carried out at FNS on a W assembly was retrieved from SINBAD database. The FNS staff developed a source routine for their generator, but the only source spectrum data in the forward direction is provided for MCNP5 analyses. It is stated that the D-energy is 350 KeV. With this set in the RDUM card, the simulation of this spectrum was attempted with the source routine. In order to reproduce also the spectrum below the peak a rough geometrical model of the target assembly (accelerator tube, radiator …) was inferred from available literature and implemented in the MCNP5 input file. The source routine allows reproducing the peak with high precision (Figure 11). The calculated signal is not broadened. A 2.5% shift in the energy scale is introduced. This is considered acceptable since the declared systematic error involved in the neutron spectrum is 4% at E>10MeV. At lower energies, the effects of structural components are somehow taken into account besides poor statistics (Figure 12). The source routine was then applied to the FNS integral experiment on W. The measured neutron spectrum at 7.6 cm inside a W block is the signal most affected by the source neutrons. Thus, it represents a good test for the source routine. A realistic model of the facility was developed for reducing the uncertainties due to the geometrical modelling. The calculated signal was broadened with a procedure explained by the experimentalist [7]. Due to the mismatch between the real Ne213 detector response function and the one used, the unfolding technique gave rise to the oscillations in the measured spectrum at ~ 8 MeV and ~ 2 MeV (Figure 13). The agreement at the peak is satisfactory. This proofs that the source routine can be used for analysing the FNG integral experiments. The results in the whole energy range of the measurements are presented in Figure 14.

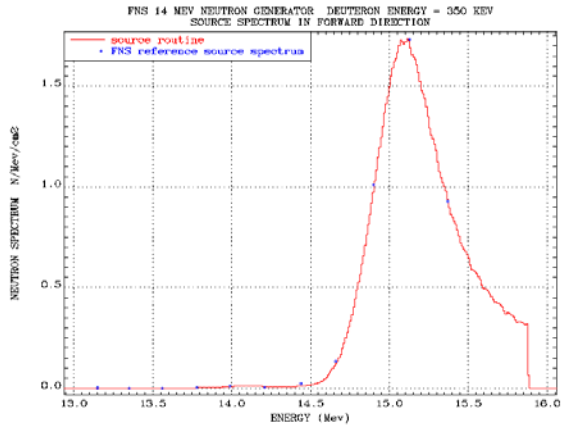

FIGURE 11. FNS neutron source peak

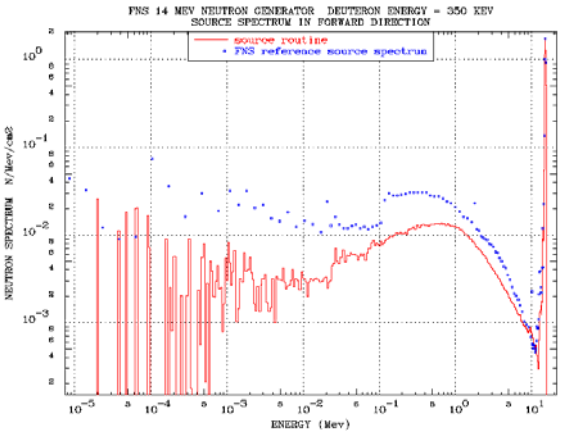

FIGURE 12. Low energy source spectrum

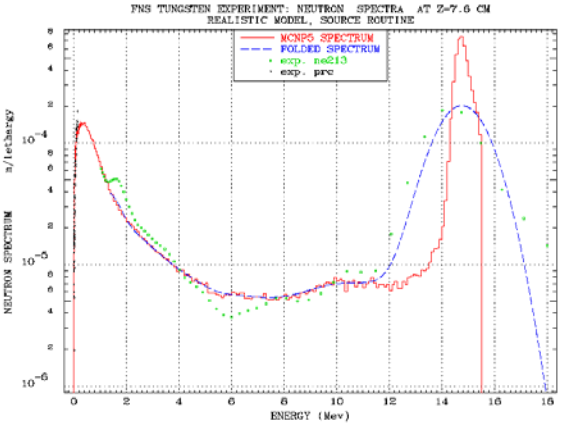

FIGURE 13. FNS W experiment, linear E scale

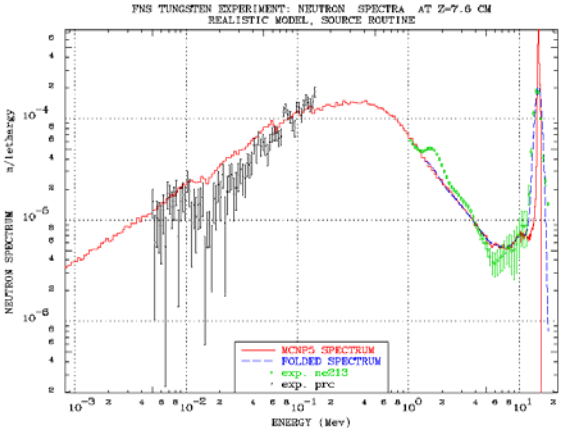

FIGURE 14. FNS W experiment, log E scale

5. Conclusions

The source routine developed at ENEA has been successfully used by the FNG team in many works and some of them are included in SINBAD. The possibility to extent its use to other neutron generators has been ascertained in the case of the FNS W experiment. The major advantage of employing the source subroutine is the reduction and separation of the uncertainties due to the source specification in MCNP5 input files. A posteriori it confirms to be efficient for the purpose. However, from a physical point of view the modelling implemented in the source routine is sometimes oversimplified and not very clear. This especially holds for the deuteron flux in the target and for the neutron production after any ion collision. It is not expected that the implementation of a more accurate physical model would modify the neutron spectra to a large extent. The source routine can be considered a reliable approach for the specification of the source spectrum in the SINBAD benchmark experiments on fusion neutronics. Experimental response functions are themselves affected by uncertainties that propagate to the final results and usually do not allow to take into account the anisotropy intrinsic to the neutron generation. The first step in using the source routine could be the calculation of the response function by arranging the parameters in the RDUM card and then simulate the integral experiment measurements with the source routine.

A. Appendix

A1. Classical and relativistic kinematics

FNG subroutine makes use of classical kinematics. The relativistic kinematics was implemented in the subroutine. The $^{3}H(d,n)^{4}He$ reaction is properly modelled as a two body reaction. Some nomenclature: in Figure 8 the subscript 'a' denotes the incident particle (deuteron), 'b' the target particle (tritium), '1' the emitted neutron and '2' the alpha particle. P and θ are the momenta and the angles between the outgoing particles and the deuteron direction, the asterisk indicated the centre–of–mass frame (CMF), T the target or laboratory frame (TF).

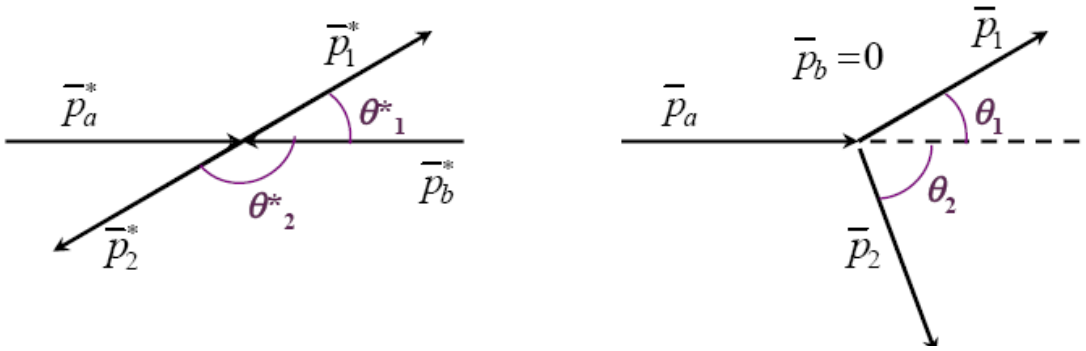

Figure A1. Two body reaction in CMF and TF

The direction of motion has been chosen as the *z* axis. Initial and final states can be expressed as follows:

CMF	TF
$p_a^*=(E_a^*,0,0,P_a^*)$	$p_a^T=(E_a^T,0,0,P_a^T)$
$p_b^*=(E_b^*,0,0,P_b^*)$	$p_b^T=(m_b,,0,0,0)$
$p_1^*=(E_1^*,0,0,P_1^*)$	$p_1^T=(E_1^T,0,0,P_1^T)$
$p_2^*=(E_b^*,0,0,P_2^*)$	$p_2^T=(E_2^T,0,0,P_2^T)$

Table 1: Particles states definition

Let's now introduce the whole set of invariant variables, the 'Mandelstam variables', s (invarant mass) and t (invariant momentum transfer), and a third variable,u, dependent on the other two.

$$s=(p_a+p_b)^2=(p_1+p_2)^2=(E_1^*+E_2^*)^2=(E_a^*+E_b^*)=m_a^2+m_b^2+2m_bE_a^T \quad (1)$$

$$t=(p_a-p_1)^2=(p_b-p_2)^2=m_a^2+m_1^2-2E_aE_1+2P_aP_1\cos\theta_{a1} \quad (2)$$

$$u=(p_a-p_2)^2=(p_b-p_1)^2=m_b^2+m_1^2-2m_bE_1^T \quad (3)$$

$$s+t+u=m_a^2+m_b^2+m_1^2+m_2^2 \quad (4)$$

In the CMF $p_a+p_b\rightarrow p_1+p_2$ is kinematically very simple, since the energy & angle dependences are completely decoupled.

$$P_a^*=P_b^*=P^* \quad (5)$$

$$\Theta_1^*=\Theta_2^*-\pi \quad (6)$$

Since:

$$E^2=P^2+m^2 \quad (7)$$

Equation (1) yields:

$$s=(E_a^*+E_b^*)^2=\left[\sqrt{P_a^{*2}+m_a^*}+\sqrt{P_b^{*2}+m_b^2}\right]^2=P^{*2}+m_a^2+P^{*2}+m_b^*+2\sqrt{\left(P^{*2}+m_a^2\right)\left(P^{*2}+m_b^2\right)} \quad (8)$$

$$s-2P^{*2}-m_a^2-m_b^2=2\sqrt{\left(P^{*2}+m_a^2\right)\left(P^{*2}+m_b^2\right)} \quad (9)$$

Squaring:

$$s^2+4P^{*4}+m_a^4+m_b^4-4sP^{*2}-2sm_a^2-2sm_b^2+4P^{*2}m_a^2+4P^{*2}m_b^2+2m_a^2m_b^2= 4P^{*4}+4P^{*2}m_a^2+4P^{*2}m_b^2+4m_a^2m_b^2 \quad (10a)$$

$$s^2-2sm_a^2-2sm_b^2-2m_a^2m_b^2+4m_a^4+4m_b^4=4sP^{*2} \quad (10b)$$

The root is:

$$P^*=\frac{\sqrt{s^2-2sm_a^2-2sm_b^2+4m_a^4+4m_b^4-2m_a^2m_b^2}}{2\sqrt{s}}=\frac{\sqrt{\left[s-(m_a+m_b)^2\right]\left[s-(m_a-m_b)^2\right]}}{2\sqrt{s}} \quad (11)$$

We introduce the kinematical function λ, which is invariant under all permutations of its arguments. It is sometimes called the triangle function.

$$\lambda(s,m_a^2,m_b^2)=\left[s-(m_a+m_b)^2\right]\left[s-(m_a-m_b)^2\right] \qquad (12)$$

So we find:

$$P_a^*=P_b^*=\sqrt{\lambda(s,m_a^2,m_b^2)}/2\sqrt{s} \qquad (13)$$

In a similar way it is possible to express all the quantities of interest in the CMF and in the TF (Table 2).

CMF	TF
$P_a^*=P_b^*=\sqrt{\lambda(s,m_a^2,m_b^2)}/2\sqrt{s}$	$P_a^T=\sqrt{\lambda(s,m_a^2,m_b^2)}/2m_b$
$P_1^*=P_2^*=\sqrt{\lambda(s,m_1^2,m_2^2)}/2\sqrt{s}$	$P_1^T=\sqrt{\lambda(u,m_b^2,m_1^2)}/2m_b$
	$P_2^T=\sqrt{\lambda(t,m_b^2,m_2^2)}/2m_b$
$E_a^*=(s+m_a^2-m_b^2)/2\sqrt{s}$	$E_a^T=(s+m_a^2-m_b^2)/2m_b$
$E_b^*=(s+m_b^2-m_a^2)/2\sqrt{s}$	
$E_1^*=(s+m_1^2-m_2^2)/2\sqrt{s}$	$E_1^T=(m_b^2-m_1^2-u)/2m_b$
$E_2^*=(s+m_2^2-m_1^2)/2\sqrt{s}$	$E_2^T=(m_b^2+m_2^2-t)/2m_b$
$\cos\theta_{a1}^*=\frac{s(t-u)+(m_a^2-m_b^2)(m_1^2-m_2^2)}{\sqrt{\lambda(s,m_a^2,m_b^2)}\sqrt{\lambda(s,m_1^2,m_2^2)}}$	$\cos\theta_{a1}^T=\frac{(s-m_a^2-m_b^2)(m_b^2-m_1^2-u)+2m_b^2)(t-m_a^2-m_1^2)}{\sqrt{\lambda(s,m_a^2,m_b^2)}\sqrt{\lambda(u,m_b^2,m_1^2)}}$
	$\cos\theta_{a2}^T=\frac{(s-m_a^2-m_b^2)(m_b^2-m_2^2-u)+2m_b^2)(u-m_a^2-m_2^2)}{\sqrt{\lambda(s,m_a^2,m_b^2)}\sqrt{\lambda(t,m_b^2,m_2^2)}}$

Table 2: Particles energies, momenta and angles

To express the neutron energy in TF (E_1) as a function of the deuteron incident energy (E_a) and the neutron emission angle (Θ_1), let us start form:

$$P_1^T = \sqrt{\lambda(u, m_b^2, m_1^2)} / 2m_b = \sqrt{\left[u - (m_b + m_1)^2\right]\left[u - (m_b - m_1)^2\right]} / 2m_b \qquad (14)$$

Squaring and arranging the terms one obtains:

$$\begin{aligned} 4m_b^2 P_1^2 &= \left[u - (m_a + m_b)^2\right]\left[u - (m_a + m_b)^2 + 4m_a m_b\right] = \\ &= \left[u - (m_a + m_b)^2\right]^2 + 4m_a m_b\left[u - (m_a + m_b)^2\right] \end{aligned} \qquad (15)$$

u as a function of P_1 and $\cos\theta_{a1}$ is given from equation *(4)*:

$$\begin{aligned} u &= m_a^2 + m_b^2 + m_1^2 + m_2^2 - s - t = \\ &= \cancel{m_a^2} + \cancel{m_b^2} + \cancel{m_1^2} + m_2^2 - \cancel{m_a^2} - \cancel{m_b^2} - 2m_b E_a - m_a^2 - \cancel{m_1^2} + 2E_a E_1 - 2P_a P_1 \cos\theta_{a1} \end{aligned} \qquad (16)$$

E_1 relates to P_1 according to its expression in Table 2 and equation *(3)*:

$$2m_b E_1 = (m_b^2 - m_1^2 - m_2^2 + m_a^2 + 2m_b E_a + 2P_a P_1 \cos\theta) \qquad (17a)$$

$$E_1 = \frac{(m_b^2 + m_1^2 - m_2^2 + m_a^2 + 2m_b E_a + 2P_a P_1 \cos\theta)}{2(m_b + E_a)} \qquad (17b)$$

Substituting E_1 in *(16)* and u in *(15)* we obtain a second order equation in P_1 in the form ax^2+bx+c. The coefficient 'a' can be determined from first term of equation *(15)*:

$$\begin{aligned} &\left[u - (m_a + m_b)^2\right] = \\ &m_2^2 + m_a^2 - 2m_b E_a - 2P_a P_1 \cos\theta - (m_a + m_b)^2 + \\ &+ \cancel{2}E_a \frac{(m_b^2 + m_1^2 - m_2^2 + m_a^2 + 2m_b E_a + 2P_a P_1 \cos\theta)}{\cancel{2}(m_b + E_a)} \end{aligned} \qquad (18)$$

Squaring it, considering and collecting the only terms in P_1^2 gives:

$$4m_b P_1^2 = 4P_a^2 P_1^2 \cos^2\theta + \frac{4E_a^2 P_a^2 P_1^2 \cos^2\theta}{(m_b + E_a)^2} - \frac{8E_a P_a^2 P_1^2 \cos^2\theta}{(m_b + E_a)} \qquad (19a)$$

$$-m_b^2 P_1^2 + P_a^2 P_1^2 \cos^2\theta\left[1 + \frac{E_a^2}{(m_b + E_a)^2} - \frac{2E_a}{(m_b + E_a)}\right] = 0 \qquad (19b)$$

$$-m_b^2 P_1^2 + P_a^2 P_1^2 \cos^2\theta\left[1-\frac{E_a}{(m_b+E_a)}\right]^2 = 0 \qquad (19c)$$

$$P_1^2\left[-m_b^2 + P_a^2\cos^2\theta\left(\frac{m_b+E_a-E_a}{(m_b+E_a)}\right)^2\right] = 0 \qquad (19d)$$

$$P_1^2\left[(m_b+E_a)^2 - P_a^2\cos^2\theta\right] = 0 \qquad (19e)$$

$$a = \left[(m_b+E_a)^2 - P_a^2\cos^2\theta\right] \qquad (20)$$

The calculation of the other terms are left for the fun of the reader.

The final result for P_1, in the form $P_1 = \frac{b \pm \sqrt{b^2-4ac}}{a}$, is:

$$P_1 = \left\{(E_a+m_b)^2 - P_a^2\cos^2\theta_1\right\}^{-1}\left[\ P_a\cos\theta_1\left\{m_b E_a + \frac{1}{2}\left(m_a^2+m_b^2+m_1^2-m_2^2\right)\right\}+\right.$$

$$\left.+\left(E_a+m_b\right)\left[\left\{m_b E_a+\frac{1}{2}\left(m_a^2+m_b^2-m_1^2-m_2^2\right)\right\}^2 - m_1^2m_2^2 - m_1^2P_a^2\sin^2\theta_1\right]^{\frac{1}{2}}\ \right] \qquad (21)$$

Where it is clear that the first term is a^{-1}.The energy of the outgoing neutron (E_1) is calculated inserting *(21)* into *(17b)*. Thus finally one obtains:

$$E_1 = \left\{(E_a+m_b)^2 - P_a^2\cos^2\theta_1\right\}^{-1}\left[\ \left(E_a+m_b\right)\left\{m_b E_a + \frac{1}{2}\left(m_a^2+m_b^2+m_1^2-m_2^2\right)\right\}+\right.$$

$$\left.+P_a\cos\theta_1\left[\left\{m_b E_a+\frac{1}{2}\left(m_a^2+m_b^2-m_1^2-m_2^2\right)\right\}^2 - m_1^2m_2^2 - m_1^2P_a^2\sin^2\theta_1\right]^{\frac{1}{2}}\ \right] \qquad (22)$$

From the previous formulas *(21)* and *(22)* it is possible to express the law for the angle relativistic transformation when passing from the CMT to the TF in the following way.

The reaction cross section for $p_a+p_b \rightarrow p_1+p_2$ is:

$$\sigma(s) = \frac{1}{8\pi^2\sqrt{\lambda(s,m_a^2,m_b^2)}}\int\frac{d^3p_1}{2E_1}\frac{d^3p_2}{2E_2}\delta^4(p_a+p_b-p_1-p_2)\left|M\right|^2 \qquad (23)$$

The matrix element M depends here on two independent variables (an invariant and an angle). Doing the integration over phase space partly, one gets (this derivation is omitted) in CMF:

$$\frac{d\sigma}{d\Omega_1^*} = \frac{|M|^2 \sqrt{\lambda(s, m_1^2, m_2^2)}}{64\pi^2 s \sqrt{\lambda(s, m_a^2, m_b^2)}} \qquad (24)$$

and in TF:

$$\frac{d\sigma}{d\Omega_1^T} = \frac{|M|^2}{64\pi^2 m_b P_a^T} \cdot \frac{(P_1^T)^2}{(E_a^T + m_b)P_1^T - P_a^T E_1^T \cos\theta_{a1}^T} \qquad (25)$$

Considering the ratio $d\Omega_{CM}/d\Omega_{LAB}$, the only part depending on the angle θ_1 is the second factor of *(25)*. All the other terms can be included in a constant *K* that is set by the normalisation.

$$\frac{d\Omega_{CM}}{d\Omega_{LAB}} = K \frac{P_1^2}{(E_a + m_b)P_1 - P_a E_1 \cos\theta_1} \qquad (26)$$

A2 The rejection method

Let us define an analytical probabibility density function (pdf), which can be very complicated. The extraction of a random variable (rv) *X* from this pdf with the rejection method consists of extrating a trial rv *X'* from a simpler pdf. This value is submitted to a test. The test requires the extraction of another rv from a uniform pdf in [0 1]. The proposed value *X'* is accepted, that is *X=X'* only if the test is passed; otherwise *X'* is rejected. In general, given $f_X(x)$ complicated, it is first split into the product of a pdf $g_{X'}(x)$, from which it is easy to extract the rv *X'*, and a residual function *H(x)*, that is:

$$f_X(x) = g_{X'}(x) H(x) \qquad (1)$$

It has to be noted that *H(x)*, being the ratio between two pdf, is not negative. Let us define B_H as:

$$B_H = \max_x H(x) = \max_x \frac{f(x)}{g_{X'}(x)} \qquad (2)$$

One gets:

$$f_X(x) = g_{X'}(x)\frac{H(x)}{B_H}B_H = g_{X'}(x)h(x)B_H \qquad (3)$$

Where:

$$h(x) = \frac{H(x)}{B_H} \quad \text{so that } 0 \le h(x) \le 1 \qquad (4)$$

Dividing by the integral of $f_X(x)$ over the whole space, for hypotesis equal to 1, one obtaines:

$$f_X(x) = \frac{g_{X'}(x)h(x)}{\int_{-\infty}^{+\infty} g_{X'}(z)h(z)dz} \qquad (5)$$

It has to be noted that from (3), integrating over all the domain of x, one obtaines:

$$\int_{-\infty}^{+\infty} g_{X'}(z)h(z)dz = \frac{1}{B_H} \qquad (6)$$

From this and from *(4)*:

$$\int_{-\infty}^{+\infty} g_{X'}(z)h(z)dz \le \int_{-\infty}^{+\infty} g_{X'}(z)dz \qquad (7)$$

As a consequence

$$B_H \ge 1$$

The extraction of a rv from $f_X(x)$ is carried out in two steps:

a) X' is extracted from pdf $g_{X'}(x)$, which is simple for construntion:

$$\Pr\{X' \le x\} = G_{X'}(x) = \int_{-\infty}^{x} g_{X'}(z)dz \qquad (8)$$

And then $h(X')$ is calculated

b) a rv R is extracted from uniform distribution between 0 and 1. If $R \le h(X')$ then X' is accepted; atherwise X' is rejected and the procedure is restarted from point a). The probability of accepting X' is:

$$\Pr\{R \le h(X')\} = h(X') \qquad (9)$$

Let us show that the accepted X is indeed extracted from $f_X(x)$.

The pdf of extracting a value X' between z and $z+dz$ and accepting this X' is given by the product of the respective probabilities:

$$\Pr\{z \le X' < z+dz\}\Pr\{R \le h(z)\} = g_{X'}(z)h(z)dz \qquad (10)$$

The corresponding cumulative density function (cdf) of extracting a value $X' \le x$ and to accept it is then:

$$\Pr\left\{X' \le x \quad AND \quad R \le h(X')\right\} = \int_{-\infty}^{x} g_{X'}h(z)h(z)dz \qquad (11)$$

The cdf that every extracted X' is accepted (the probability of full success) is the marginal distribution with respect of X' from (8), that is:

$$\Pr\{success\} = \Pr\left\{X' < \infty \quad AND \quad R \le h(X')\right\} = \int_{-\infty}^{+\infty} g_{X'}(z)h(z)dz \qquad (12)$$

Let us consider now the cdf of the only accepted values (the others are rejected): it yields:

$$\Pr\{X' \le x | success\} = \frac{\Pr\left\{X' \le x \quad AND \quad R \le h(X')\right\}}{\Pr\{success\}} = \frac{\int_{-\infty}^{x} g_{X'}(z)h(z)dz}{\int_{-\infty}^{+\infty} g_{X'}(z)h(z)dz} \qquad (13)$$

And the corresponding pdf is (5) that is the assigned $f_X(x)$.

The simple version of Von Neumanns's rejection method is the particular case in which

$$g_{X'}(x) = \frac{1}{b-a} \qquad (14)$$

That is a uniform distribution between a and b. In the source routine the variable x is the polar angle of neutron emission in the CM system. It is first extracted from a uniform distribution between cosine -1 and cosine 1, as usual. The maximum value of the double differential cross sections over all angles and energies is found and a rv extracted between 0 and 1 is compared with h(x'), thus performing the test. This discussion on the rejection method refers to a

monovariate pdf. The cross sections in the source routine is bi-dimentional. Since the D energy is fixed, the discussion above holds in this case too. One can argue that the maximum value of the angular distributions should be selected according to the sampled value of the emission angle. To this purpose, different maxima were calculated for different energies and, after extraction of the emission angle, the nearest value was obtained by interpolation and set as h(X'). The effect of this refinement can be assessed from Figure A2. No important difference is noticeable.

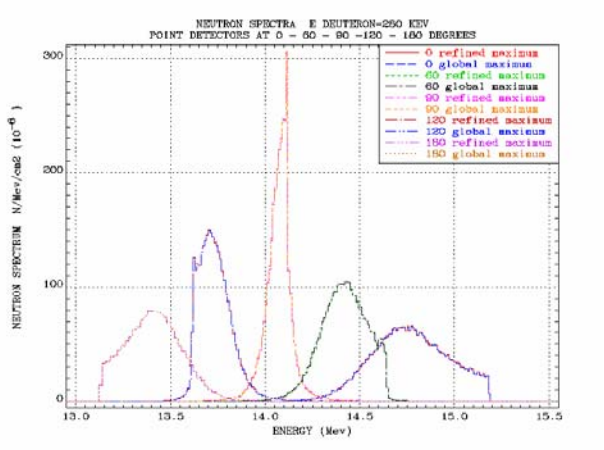

Figure A2. Effect of rejection method refinement

References

[1] *J. F. Ziegler, J. P. Biersack and M. D. Ziegler*:'SRIM - THE STOPPING AND RANGE OF IONS IN MATTER', SRIM co. 2008

[2] *M.R.C. McDowell, J.P Coleman*: 'INTRODUCTION TO THE THEORY OF ION-ATOM COLLISIONS', North-Holland publishing company, Amsterdam-London, 1970

[3] *M. Drosg*: 'MONOENERGETIC NEUTRON PRODUCTION BY TWO BODY REACTIONS IN THE ENERGY RANGE FROM 0.0001 TO 500 MEV', TCM-Meeting of IAEA, Debrecen, Hungary, 1999.

[4] *Cross Section Evaluation Working Group*: 'ENDF - 6 FORMATS MANUAL', Brookhaven National Laboratory, Report BNL - NCS - 44945 - 05 - Rev., Upton, N. Y., April 2004, pp H – 4

[5] *M. Angelone, M. Pillon, P. Batistoni, M. Martini, M. Martone and V. Rado*: 'ABSOLUTE EXPERIMENTAL AND NUMERICAL CALIBRATION OF THE 14 MEV NEUTRON SOURCE AT THE FRASCATI NEUTRON GENERATOR', Rev. Sci. Instrum. 67 (6), June 1996

[6] *M. Pillon, M. angelone, A.V Krasilnikov*:'14 MEV SPECTRA NEASUREMENTS WITH 4% ENERGY RESOLUTION USING A TYPE IIA DIAMOND DETECTOR', Nuclear Instruments and Methods in Physical Research B 101 (1995) 473-483

[7] *F. Maekawa, C. Konno, Y. Kasugai, Y. Oyama, Y. Ikeda*:'DATA COLLECTION OF FUSION NEUTRONICS BENCHMARK EXPERIMENT CONDUCTED AT FNS/JAERI', JAERI-Data/Code 98-021 (1998)